$$H_{Bionic}(f) = \frac{H_{Naive}(f)}{H_{Stim \to AP}(f)} \quad \text{(B5)}$$

After determining the transfer function of the bionic baroreflex, we obtained the impulse response of the bionic baroreflex system [$h_{Bionic}(\tau)$] via inverse Fourier transform of the transfer function. We then calculated the stimulus command [$c_{Stim}(t)$] from the convolution integral between $h_{Bionic}(\tau)$ and baroreceptor pressure input [$p_{Input}(t)$] according to the following equation.

$$c_{Stim}(t) = \int_0^T h_{Bionic}(\tau) p_{Input}(t-\tau) d\tau \quad \text{(B6)}$$

In the above convolution integral, $p_{Input}(t)$ was treated as the change in arterial pressure from the arterial pressure value measured immediately before hypotensive intervention.

Acknowledgments

Supported in part by "Health and Labour Sciences Research Grant for Research on Advanced Medical Technology", "Health and Labour Sciences Research Grant for Research on Medical Devices for Analyzing, Supporting and Substituting the Function of Human Body", "Health and Labour Sciences Research Grant", from the Ministry of Health, Labour and Welfare of Japan.

References

1. Dowling J. Artificial human vision. Expert Rev Med Devices 2005;2:73-85
2. Walter P, Kisvárday ZF, Görtz M, Alteheld N, Rossler G, Stieglitz T, Eysel UT. Cortical activation via an implanted wireless retinal prosthesis. Invest Ophthalmol Vis Sci 2005;46(5):1780-1785
3. Papsin BC, Gordon KA. Cochlear implants for children with severe-to-profound hearing loss. N Engl J Med 2007;357:2380-2387
4. Lim HH, Lenarz T, Joseph G, Battmer RD, Samii A, Samii M, Patrick JF, Lenarz M. Electrical stimulation of the midbrain for hearing restoration: insight into the functional organization of the human central auditory system. J Neurosci 2007;27:13541-13551
5. Mushahwar VK, Jacobs PL, Normann RA, Triolo RJ, Kleitman N. New functional electrical stimulation approaches to standing and walking. J Neural Eng 2007;4(3):S181-S197
6. Sujith OK. Functional electrical stimulation in neurological disorders. Eur J Neurol. 2008; 15:437-444.
7. Ikeda Y, Sugimachi M, Yamasaki T, Kawaguchi O, Shishido T, Kawada T, Alexander J Jr, Sunagawa K. Explorations into development of a neurally regulated cardiac pacemaker. Am J Physiol 1995;269:H2141-H2146
8. Berger RD, Saul JP, Cohen RJ. Transfer function analysis of autonomic regulation. I. Canine atrial rate response. Am J Physiol 1989; 256:H142-H152
9. Miyano H, Nakayama Y, Shishido T, Inagaki M, Kawada T, Sato T, Miyashita H, Sugimachi M, Alexander J Jr, Sunagawa K. Dynamic sympathetic regulation of left ventricular contractility studied in the isolated canine heart. Am J Physiol 1998;275:H400-H408
10. Kawada T, Uemura K, Kashihara K, Jin Y, Li M, Zheng C, Sugimachi M, Sunagawa K. Uniformity in dynamic baroreflex regulation of left and right cardiac sympathetic nerve activities. Am J Physiol Regul Integr Comp Physiol 2003; 284:R1506-R1512
11. Parikh SM, Diedrich A, Biaggioni I, Robertson D. The nature of the autonomic dysfunction in multiple system atrophy. J Neurol Sci 2002; 200:1-10
12. Sato T, Kawada T, Shishido T, Sugimachi M, Alexander J Jr, Sunagawa K. Novel therapeutic strategy against central baroreflex failure: a bionic baroreflex system. Circulation 1999;100:299-304

13. Sato T, Kawada T, Sugimachi M, Sunagawa K. Bionic technology revitalizes native baroreflex function in rats with baroreflex failure. Circulation 2002;106:730-734
14. Yanagiya Y, Sato T, Kawada T, Inagaki M, Tatewaki T, Zheng C, Kamiya A, Takaki H, Sugimachi M, Sunagawa K. Bionic epidural stimulation restores arterial pressure regulation during orthostasis. J Appl Physiol 2004;97:984-990
15. Yamasaki F, Ushida T, Yokoyama T, Ando M, Yamashita K, Sato T. Artificial baroreflex: clinical application of a bionic baroreflex system. Circulation 2006;113:634-639
16. Gotoh TM, Tanaka K, Morita H. Controlling arterial blood pressure using a computer-brain interface. Neuroreport 2005;16:343-347
17. Mudd JO, Kass DA. Tackling heart failure in the twenty-first centry. Nature 2008;451:919-928
18. Li M, Zheng C, Sato T, Kawada T, Sugimachi M, Sunagawa K. Vagal nerve stimulation markedly improves long-term survival after chronic heart failure in rats. Circulation 2004;109:120-124
19. Nakayama Y, Miyano H, Shishido T, Inagaki M, Kawada T, Sugimachi M, Sunagawa K. Heart rate-independent vagal effect on end-systolic elastance of the canine left ventricle under various levels of sympathetic tone. Circulation. 2001;104:2277-2279
20. Vanoli E, De Ferrari GM, Stramba-Badiale M, Hull SS Jr, Foreman RD, Schwartz PJ. Vagal stimulation and prevention of sudden death in conscious dogs with a healed myocardial infarction. Circ Res 1991;68:1471-181
21. Kawada T, Yamazaki T, Akiyama T, Li M, Ariumi H, Mori H, Sunagawa K, Sugimachi M. Vagal stimulation suppresses ischemia-induced myocardial interstitial norepinephrine release. Life Sci. 2006;78:882-887
22. Rona G. Catecholamine cadiotoxicity. J Mol Cell Cardiol 1985;17:291-306.
23. Uemura K, Li M, Tsutsumi T, Yamazaki T, Kawada T, Kamiya A, Inagaki M, Sunagawa K, Sugimachi M. Efferent vagal nerve stimulation induces tissue inhibitor of metalloproteinase-1 in myocardial ischemia-reperfusion injury in rabbit. Am J Physiol Heart Circ Physiol 2007;293:H2254-H2261
24. Kawada T, Yamazaki T, Akiyama T, Sato T, Shishido T, Inagaki M, Takaki H, Sugimachi M, Sunagawa K. Differential acetylcholine release mechanisms in the ischemic and non-ischemic myocardium. J Mol Cell Cardiol 2000;32:405-414

25. Kawada T, Yamazaki T, Akiyama T, Uemura K, Kamiya A, Shishido T, Mori H, Sugimachi M. Effects of Ca^{2+} channel antagonists on nerve stimulation-induced and ischemia-induced myocardial interstitial acetylcholine release in cats. Am J Physiol Heart Circ Physiol 2006;291:H2187-H2191
26. Zheng C, Kawada T, Li M, Sato T, Sunagawa K, Sugimachi M. Reversible vagal blockade in conscious rats using a targeted delivery device. J Neurosci Methods 2006; 156:71-75
27. Marmarelis PZ, Marmarelis VZ. Analysis of Physiological Systems. The white noise method in system identification. New York: Plenum, 1978, p. 131-221.

Figure 1

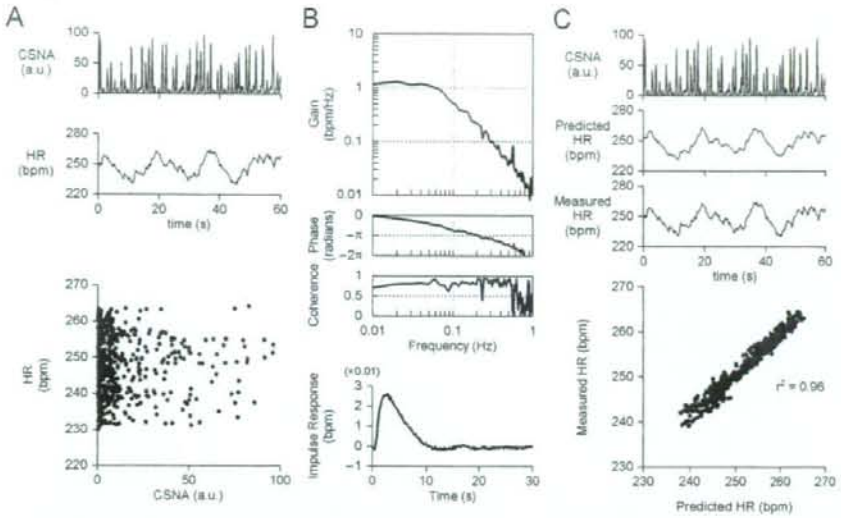

Decoding of sympathetic heart rate control (see Ref 7). A: Recordings of cardiac sympathetic nerve activity (CSNA) and heart rate (HR), which were plotted against each other. B: Transfer function from CSNA to HR and the corresponding impulse response. C: Prediction of HR from CSNA using the transfer function. A scatter plot of measured HR versus predicted HR displays the accuracy of this prediction.

Figure 2

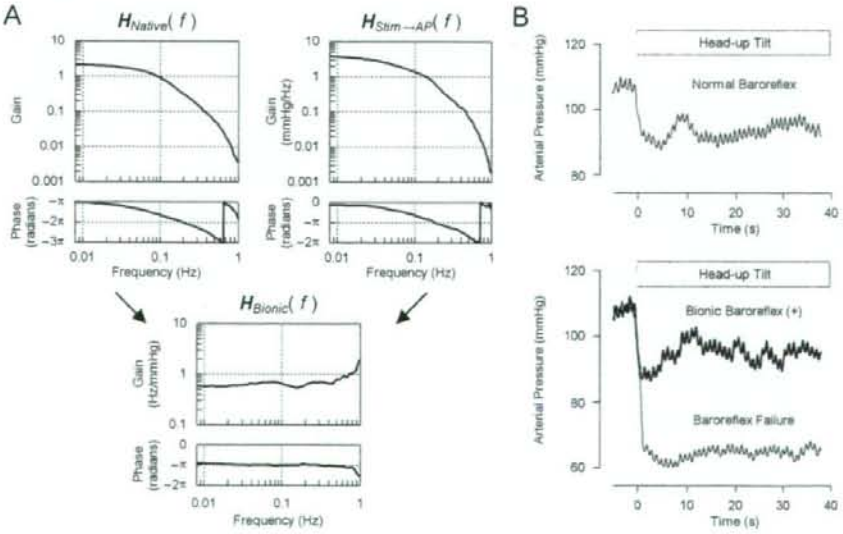

Arterial pressure regulation by the bionic baroreflex system (See Ref 13). A: Transfer function of the native baroreflex [$H_{Native}(f)$], transfer function from stimulation of the celiac ganglion to arterial pressure [$H_{Stim \rightarrow AP}(f)$], and transfer function of the bionic baroreflex [$H_{Bionic}(f)$]. B: Arterial pressure responses during head-up tilt in the rat with normal baroreflex (top) and in the rat with central baroreflex failure (bottom). Activation of the bionic baroreflex system restored the buffering effect against orthostatic hypotension.

Figure 3

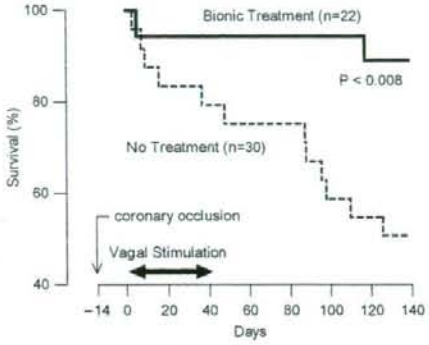

Survival of rats with chronic heart failure after myocardial infarction (see Ref 18). Vagal stimulation dramatically improved the survival rate.

Annals of Biomedical Engineering, Vol. 37, No. 1, January 2009 (© 2008) pp. 112–128
DOI: 10.1007/s10439-008-9599-4

Wavelet-Based System Identification of Short-Term Dynamic Characteristics of Arterial Baroreflex

KOJI KASHIHARA,[1,2] TORU KAWADA,[3] MASARU SUGIMACHI,[3] and KENJI SUNAGAWA[4]

[1]Hypertension and Stroke Research Laboratory, Royal North Shore Hospital, University of Sydney, Ground Floor, Building 10, Royal North Shore Hospital, St. Leonards, NSW 2065, Australia; [2]National Institute for Longevity Sciences, NCGG, 36-3 Gengo, Morioka-machi, Obu City, Aichi 474-8511, Japan; [3]Department of Cardiovascular Dynamics, National Cardiovascular Center Research Institute, 5-7-1 Fujishirodai, Suita, Osaka 565-8565, Japan; and [4]Department of Cardiovascular Medicine, Kyushu University, 3-1-1, Maidashi, Higashi-ku, Fukuoka 812-8582, Japan

(Received 1 February 2008; accepted 31 October 2008; published online 12 November 2008)

Abstract—The assessment of arterial baroreflex function in cardiovascular diseases requires quantitative evaluation of dynamic and static baroreflex properties because of the frequent modulation of baroreflex properties with unstable hemodynamics. The purpose of this study was to identify the dynamic baroreflex properties from transient changes of step pressure inputs with background noise during a short-duration baroreflex test in anesthetized rabbits with isolated carotid sinuses, using a modified wavelet-based time-frequency analysis. The proposed analysis was able to identify the transfer function of baroreflex as well as static properties from the transient input-output responses under normal [gain at 0.04 Hz from carotid sinus pressure (CSP) to arterial pressure ($n = 8$); 0.29 ± 0.05 at low (40–60 mmHg), 1.28 ± 0.12 at middle (80–100 mmHg), and 0.38 ± 0.07 at high (120–140 mmHg) CSP changes] and pathophysiological [gain in control vs. phenylbiguanide ($n = 8$); 0.32 ± 0.07 vs. 0.39 ± 0.09 at low, 1.39 ± 0.15 vs. 0.59 ± 0.09 ($p < 0.01$) at middle, and 0.35 ± 0.04 vs. 0.15 ± 0.02 ($p < 0.01$) at high CSP changes] conditions. Subsequently, we tested the proposed wavelet-based method under closed-loop baroreflex responses; the simulation study indicates that it may be applicable to clinical situations for accurate assessment of dynamic baroreflex function. In conclusion, the dynamic baroreflex property to various pressure inputs could be simultaneously extracted from the step responses with background noise.

Keywords—Baroreceptor reflex, Sympathetic nerve activity, Arterial pressure, Transfer function, Dynamic characteristics.

INTRODUCTION

Arterial baroreflex is a crucial negative feedback system because of the quick stabilization of arterial pressure (AP) against external pressure disturbances.[12,30] The assessment of arterial baroreflex function would require quantifying the dynamic as well as static properties[15,46] because the baroreflex gain or sensitivity is frequently modulated during cardiovascular diseases.[6,36,39] Because quick responses of autonomic nerves and AP mainly through the brainstem[3] might contain the unknown characteristics changing by the minute in acute cardiovascular diseases,[25] the short-term dynamic system identification might relate to the novel finding under such nonstationary condition. Laboratory and spontaneous baroreflex methods[37] are widely used in human and animal studies. The laboratory method requires invasive pharmacological or mechanical pressure interventions, and it may be suitable for estimation of the mechanism of AP regulation through the sympathetic as well as vagal baroreflex.[7,45] The spontaneous baroreflex method aims to assess cardiovagal activity noninvasively using systolic AP and heart rate variability.[5] These methods have various merits under the baroreflex testing conditions, but remain debatable because of complicated mechanisms.[27,37,40,43]

In the laboratory method, the standard analysis of sympathetic baroreflex has been performed mainly in the time[10,16] or frequency domain.[1,29,35,44] The time-domain analysis has evaluated the stable or maximal gain around the operating point, but may not characterize the impaired dynamic baroreflex properties accurately in cardiovascular patients with unstable hemodynamics and background noise. In the frequency domain, fast Fourier transform (FFT) analysis[31] has identified dynamic baroreflex properties under such noisy condition, but requires longer data segments to cancel the background noise and to identify the dynamic properties with low-frequency band,[38] indicating difficulties to extract short-term changes. In

Address correspondence to Koji Kashihara, Hypertension and Stroke Research Laboratory, Royal North Shore Hospital, University of Sydney, Ground Floor, Building 10, Royal North Shore Hospital, St. Leonards, NSW 2065, Australia. Electronic mail: kojikasi-nils@umin.ac.jp

the spontaneous baroreflex method, the analytical time window based on short-time FFT[5] (STFFT) has been adjusted to evaluate the time-varying gain around the operating point. However, this method may not be suitable for the evaluation of short-term changes in baroreflex properties for AP regulation through sympathetic as well as vagal nerves, at multiple pressure points with background noise. A combination of time and frequency analysis using wavelet transform may be able to identify the dynamic baroreflex properties efficiently regardless of background noise[2,4] by virtue of its high temporal resolution.[34] If dynamic and static characteristics in cardiovascular patients with unstable hemodynamics can be identified in a short-duration baroreflex test, various pathophysiological characteristics may be gained simultaneously.

The first purpose of this study was to examine whether a proposed wavelet-based time-frequency analysis was able to identify the dynamic as well as static baroreflex properties in animals from transient step pressure inputs with background noise during a short-duration test. Next, the proposed analysis was applied to identify unknown dynamic baroreflex properties in nonlinear AP input ranges during the Bezold-Jarisch reflex (BJR). We hypothesized that the proposed analysis could evaluate the baroreflex transfer properties from a short-term protocol, simultaneously at various pressure inputs under normal and BJR conditions. Finally, we examined the possibility of applying the new analysis to human studies to evaluate the dynamic baroreflex for AP regulation through the sympathovagal activity.

METHODS

Pathways of Baroreflex Functions

Under the carotid sinus open-loop condition, we defined the total loop as the system from carotid sinus pressure (CSP) input to AP output, which is divided into the neural arc as the subsystem from CSP input to renal sympathetic nerve activities (RSNA) output and the peripheral arc as the subsystem from RSNA input to AP output.[15] The cardiac baroreflex was defined as the system from CSP to heart rate (HR) response,[52] which may represent sympathovagal control of the heart through the baroreflex.

Surgical Preparations

Animals were cared for in accordance with the *Guiding Principles for the Care and Use of Animals in the Field of Physiological Sciences* approved by the Physiological Society of Japan. Japanese white rabbits were anesthetized with an intravenous injection (2 mL/kg) of a mixture of urethane (250 mg/mL) and α-chloralose (40 mg/mL) followed by a continuous administration (0.2–0.3 mL/kg/h, i.v.). The rabbits were artificially ventilated with oxygen-enriched room air at 0.6 Hz. Raw wave of AP was measured from the right femoral artery, using a high-fidelity pressure transducer (Millar Instruments, Houston, TX). A double-lumen catheter was placed into the right femoral vein for drug administration. The aortic depressor nerves identified by arterial pulse-synchronous activities were sectioned, while bilateral vagi were kept intact. Bilateral carotid sinuses were isolated from the systemic circulation by ligating the external and internal carotid arteries, and were filled with warm physiological saline through catheters inserted into the common carotid arteries. CSP was adjusted with a servo-controlled piston pump controlled by a computer system.

The left renal sympathetic nerve was exposed and a pair of stainless steel wire electrodes (Bioflex wire AS633, Cooner Wire) was attached. The nerve fibers distal to the electrodes were crushed by tight ligature to eliminate afferent signals from the kidney, and were covered in silicone gel (Semicosil 932A/B, Wacker Silicones). The preamplified nerve signal, band-pass filtered at 150–1000 Hz, was full-wave rectified and low-pass filtered at a cutoff frequency of 30 Hz (i.e. Op-amp RC integrator) to quantify nerve activity. Pancuronium bromide (0.3 mg/kg, i.v.) was administered to prevent muscular activity. The body temperature was kept at 38 °C.

Step Input Protocol

The carotid sinus baroreflex negative feedback loop was closed by adjusting CSP to AP level for 20 min after the surgical preparations (8 rabbits weighing 2.7–3.0 kg). The feedback loop was then opened and CSP was maintained at 40 mmHg for 4 min until the AP response reached a steady state. CSP was then increased from 40 to 160 mmHg in increments of 20 mmHg every minute (CSP_{40-60}, CSP_{60-80}, CSP_{80-100}, $CSP_{100-120}$, $CSP_{120-140}$, and $CSP_{140-160}$ changes). The single trial was repeated three times every rabbit. Data were sampled at 200 Hz and were averaged every 40 points for analysis (i.e. pulsatile AP signals were averaged every 0.2 s). HR (beats/min) was counted from the pulse waves of raw AP signals, which are well known as waves synchronized with ECG.[33] RSNA data of each animal were presented in arbitrary units (a.u.), with 1-min averaged background noise taken as zero level and 10-s averaged RSNA at CSP of 40 mmHg in normal condition set as unity.

Data Analysis

Identification of Dynamic Baroreflex

After the recorded data (three times) of CSP, RSNA, AP and HR were averaged in each animal, the signals were convoluted by complex Morlet wavelet, $w(t, f_0)$:[48,49]

$$w(t, f_0) = \frac{1}{\sqrt{\sigma_t\sqrt{\pi}}} \cdot \exp\left(\frac{-t^2}{2\sigma_t^2}\right) \cdot \exp(2\pi f_0 it) \qquad (1)$$

where the $(\sigma_t\sqrt{\pi})^{-1/2}$ normalizes the wavelets to be unity total energy, and the $\exp(-t^2/2\sigma_t^2)$ is a Gaussian shape with the central frequency f_0 at time t. The standard deviation (σ_t) of the time domain is inversely proportional to the standard deviation (σ_f) of the frequency domain [$\sigma_f = (2\pi\sigma_t)^{-1}$]. A constant ratio, f_0/σ_f, determines the effective number of oscillation cycles in the wavelet. The f_0/σ_f was determined[11] as 5 with f_0 ranging from 0.04 to 0.4 Hz[32] in increments of 0.01 Hz. Because the dynamic baroreflex function was well characterized by the transfer function up to around 0.4 Hz based on the corner frequency and slope of gain change,[15,32] the upper frequency limit for analysis was set at 0.4 Hz, considering also the limitation of the step input (low power in high frequency components) and the respiratory frequency of 0.6 Hz. The wavelet duration ($2\sigma_t$) is 39.8 s at 0.04 Hz and 3.98 s at 0.4 Hz, and the spectral band width ($2\sigma_f$) is 0.016 Hz at 0.04 Hz and 0.16 Hz at 0.4 Hz.

The linear trend was subtracted only in animal study, and the continuous wavelet transform of time series $u(t)$ was calculated as the convolution of a complex wavelet [$w(t, f_0)$] with the $u(t)$:

$$\tilde{u}(t, f_0) = w(t, f_0) * u(t) \qquad (2)$$

The power $P(t, f_0)$ of the signal in a frequency band at around f_0 is the squared norm of the wavelet transform: $P(t, f_0) = |\tilde{u}(t, f_0)|^2$. The symbol (*) shows the convolution in the time domain

To identify the dynamic baroreflex property from time-sequential data, we define the transfer function [$H(t, f_0)$] from input to output using wavelet transform as follows.

$$H(t, f_0) = \frac{P_{xy}(t, f_0)}{P_{xx}(t_{\text{event}}, f_0)} \qquad (3)$$

where

$$\begin{cases} P_{xx}(t_{\text{event}}, f_0) = \tilde{x}(t_{\text{event}}, f_0) \cdot \tilde{x}^{\oplus}(t_{\text{event}}, f_0) \\ P_{xy}(t, f_0) = \tilde{x}(t_{\text{event}}, f_0) \cdot \tilde{y}^{\oplus}(t, f_0) \end{cases}$$

$P_{xx}(t_{\text{event}}, f_0)$ is the auto-wavelet spectrum of the input signal [$x(t)$] with central frequency f_0 at a fixed time t_{event} when the power is maximum. The t_{event} shows the sole value of the analysis time (t) at f_0; the transfer function shows the effect of the maximum input power at t_{event} on the output responses during analysis time, t, for every f_0. Here, we used the fixed input value to extract the dynamics strictly against the step input. The cross-wavelet spectrum, $P_{xy}(t, f_0)$, which is an effective way to detect large-amplitude time-localized events,[26] is the convolution of the wavelet transform values of the input-output signals [$\tilde{x}(t_{\text{event}}, f_0)$ and $\tilde{y}^{\oplus}(t, f_0)$]. $\tilde{x}^{\oplus}(t_{\text{event}}, f_0)$ and $\tilde{y}^{\oplus}(t, f_0)$ is the complex conjugate of $x(t_{\text{event}}, f_0)$ and $y(t, f_0)$. The segment for wavelet transform analysis was set at ±30 s of the time of the step input change and was moved to the next area of the step input. The symbol (·) shows the product in the frequency domain, which corresponds to the convolution in the time domain.

To visualize the time-series transfer function during the analysis time (t), the dynamic gain [$|H(t, f_0)| = \sqrt{H_{\text{Re}}(t, f_0)^2 + H_{\text{Im}}(t, f_0)^2}$, where $H_{\text{Re}}(t, f_0)$ and $H_{\text{Im}}(t, f_0)$ are the real and imaginary parts of $H(t, f_0)$] and phase $\left[\varphi(t, f_0) = \tan^{-1}\frac{H_{\text{Im}}(t, f_0)}{H_{\text{Re}}(t, f_0)}\right]$ of the transient transfer function during analysis time were calculated from Eq. (3).

Next, we constructed the bode plot using the maximum dynamic gains, which reflects the maximum values of input and output powers. The phase of Eq. (3) is based on the maximum $P_{xx}(t_{\text{event}}, f_0)$ as the auto-wavelet spectrum of the input signal without the lag time of system response. To calculate the phase of the bode plot, we estimated the lag time of the system response as follows:

$$\hat{L} = t_{Pxy\max} - t_{Pxx\max}, \qquad (4)$$

where $\hat{L}$ is the mean value between 0.35 and 0.4 Hz of f_0. The data between 0.35 and 0.4 Hz (5 points) were averaged because of the varied estimation. The analysis time was set to 0–6 s and the phase unwrap process to make it continuous across 2π phase discontinuities by adding multiples of $\pm 2\pi$ was applied. $t_{Pxx\max}$ is the time at the maximum auto power spectrum of the input data; $t_{Pxy\max}$ is the time at the maximum cross power spectrum of input-output data. Using the estimated lag time (L) of the system response, the phase [$\varphi(t_{\max}, f_0)$] of the transient transfer function is shown as follows:

$$\varphi(t_{\max}, f_0) = \tan^{-1}\frac{H'_{\text{Im}}(t_{\max}, f_0)}{H'_{\text{Re}}(t_{\max}, f_0)} \qquad (5)$$

where

$$H'(t_{\max}, f_0) = H(t_{\max}, f_0) \cdot \exp(-2\pi f_0 iL)$$

$H'_{Re}(t_{max}, f_0)$ and $H'_{Im}(t_{max}, f_0)$ are the real and imaginary parts of $H'(t_{max}, f_0)$ with lag time, L. t_{max} is the time when the dynamic gain is maximum.

Static Characteristics

After the RSNA, AP, and HR during the last 10 s of each CSP level were averaged using the data of the step-input protocol, the static characteristics of total baroreflex loop, neural arc, and cardiac baroreflex control were examined by regression analysis for the logistic function.[24,46,47] To quantify static characteristics of the peripheral arc, linear regression analysis was performed. The closed-loop operating point of the baroreflex (AP_{OP}) was determined from the intersection point between the CSP-AP curve (total baroreflex loop) and CSP-AP identity line. AP_{OP} was also determined from AP at the intersection point between the CSP-RSNA curve (neural arc) and RSNA-AP line (peripheral arc) in the equilibrium diagram.[18]

Standard Analysis

The STFFT as a traditional time-frequency method was applied to the step-input (±20 mmHg) protocol, using the model response between CSP and AP (see Appendix). The time window was set to 12.8 s (64 data points) and 51.2 s (256 points, which is close to that at the lowest frequency in the used wavelet method). After the application of the detrend and Hanning window, power spectral densities of the CSP and AP and the transfer gain of the cross-spectra were computed every 200 ms. In the STFFT (256 points), pseudo-random noises were added to the input (within ±0.1 mmHg) and output (±1 mmHg every 200 ms) signals. The STFFT analysis was also compared with the proposed wavelet analysis over frequencies under the pseudo-random noise within ±0.1 mmHg in the input and ±1 or ±2 mmHg in output every 200 ms.

Experiment of Bezold-Jarisch Reflex

To elucidate the modified wavelet-based analysis in the pathophysiological condition, the previous datasets assessing static baroreflex during BJR[18] were reanalyzed; the data at sampling rate of 200 Hz were averaged every 40 points. In 8 anesthetized rabbits with sectioned aortic depressor nerves, intact vagi, and isolated carotid sinuses, CSP was increased stepwise while AP and HR were recorded before and after 7-min administration of a serotonin ($5\text{-}HT_3$) receptor agonist, phenylbiguanide (PBG, 100 μg/kg/min, intravenous infusion): Control and PBG conditions. Vagal afferent was confirmed as the main pathway of the BJR induced by intravenous PBG infusion.[20]

Cardiac Baroreflex

The role of cardiac baroreflex (CSP to HR response) was studied, focusing on the contribution of the cardiac sympathovagal activity to dynamic baroreflex for AP regulation. The ratio of the transfer functions between cardiac baroreflex and total (CSP-AP) loop was calculated under Control and PBG conditions, using the results from the proposed analysis.

Statistical Analysis

All data are expressed as mean ± SEM. The gain, power, and frequency in the figures are shown in log scales. The transfer functions in the neural and peripheral arcs were normalized in each animal so that the average gain in all stepwise changes of normal condition became unity at 0.04 Hz. To test the difference among six stepwise changes or between the Control and PBG conditions, we obtained the gain at 0.04 ($G_{0.04}$), the average slope of the gains between 0.1 to 0.4 Hz (Slope), and the lag time in each animal. One-way analysis of variance with multiple comparisons using Bonferroni correction[9] was applied to assess the level differences. Differences were considered statistically significant at $p < 0.05$.

Simulation for Closed-Loop Baroreflex

The carotid sinus open-loop animal experiment should be linked to human closed-loop baroreflex to explore the possibility of applying the proposed analysis to clinical diagnosis. We performed a simulation study, using the emulated cardiac baroreflex model from observed AP input to observed HR output under the closed-loop AP response (see Appendix) to test the accuracy of the proposed wavelet-based analysis and to acquire the transfer functions of the cardiac baroreflex for use in human laboratory test.

RESULTS

Test of Wavelet Analysis

The proposed wavelet-based analysis was tested using the baroreflex model response between CSP and AP under carotid sinus open-loop condition (see Appendix). After the calculation of the wavelet power spectrum for the input and the input-output cross spectrum (Fig. 2a), the transfer function was acquired (Fig. 2b). The gains reached the maximum immediately after the step input at 60 s and the phase changed greatly when approaching the maximum gain. Bode plots were extracted from the maximum points of the time-course transfer function with and without

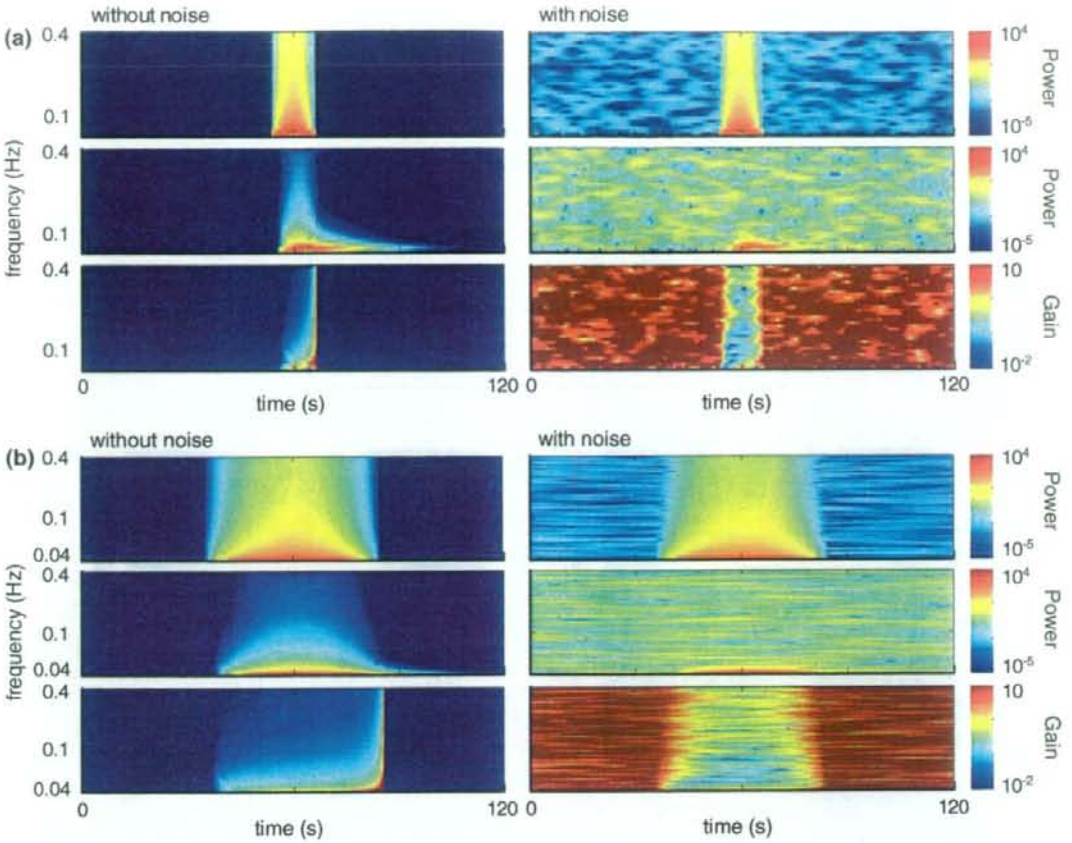

FIGURE 1. Time-frequency method based on the short-time FFT for system identification using the simulated step-input protocol. Time windows, 12.8 s (a) and 51.2 s (b). Power spectral densities of carotid sinus pressure (CSP) input (*top*) and arterial pressure (AP) output (*middle*) and transfer gain (*bottom*) in the absence (*left*) or presence (*right*) of pseudo-random noises.

background noise (Fig. 2c). In the presence of pseudo-random noise (within ±0.01 mmHg in input and ±1 mmHg in output changed every 200 ms), the transfer function closely resembled the theoretical values. Compared to the STFFT (Fig. 1), the proposed wavelet method could accurately estimate the transfer function over different frequencies, regardless of a poor signal to noise (S/N) ratio at higher frequency, because of the property of the step input power (Fig. 2d).

Dynamic Baroreflex

The averaged RSNA, AP, and HR responses to the step-input changes were decreased with the increments in CSP from 40 to 160 mmHg every minute ($n = 8$, Fig. 3a). In the averaged time series ($n = 8$, Fig. 3b), the power spectrums at all step inputs were the same values at each frequency level because of a constant change of +20 mmHg (greater in low frequency and smaller in high frequency). The powers of RSNA, AP, and HR change were higher at CSP_{80-100} than other CSP changes over all frequency ranges, and the magnitudes were especially small at low or high CSP changes.

The averaged ($n = 8$) time series of transfer functions in the neural arc (a), peripheral arc (b), total loop (c) and cardiac baroreflex (d) were calculated after wavelet transform (Fig. 4). In the neural arc, gain values in low frequencies were much less at CSP changes away from the operating point. In the peripheral arc, low pass characteristics in the gains were observed at all CSP changes except the lowest CSP_{40-60} change reflecting spontaneous neural firing. In the total baroreflex loop, the gains at CSP changes within 60–120 mmHg were higher than those at other CSP changes, indicating low-pass characteristics. In the cardiac baroreflex, the gains were smaller at the

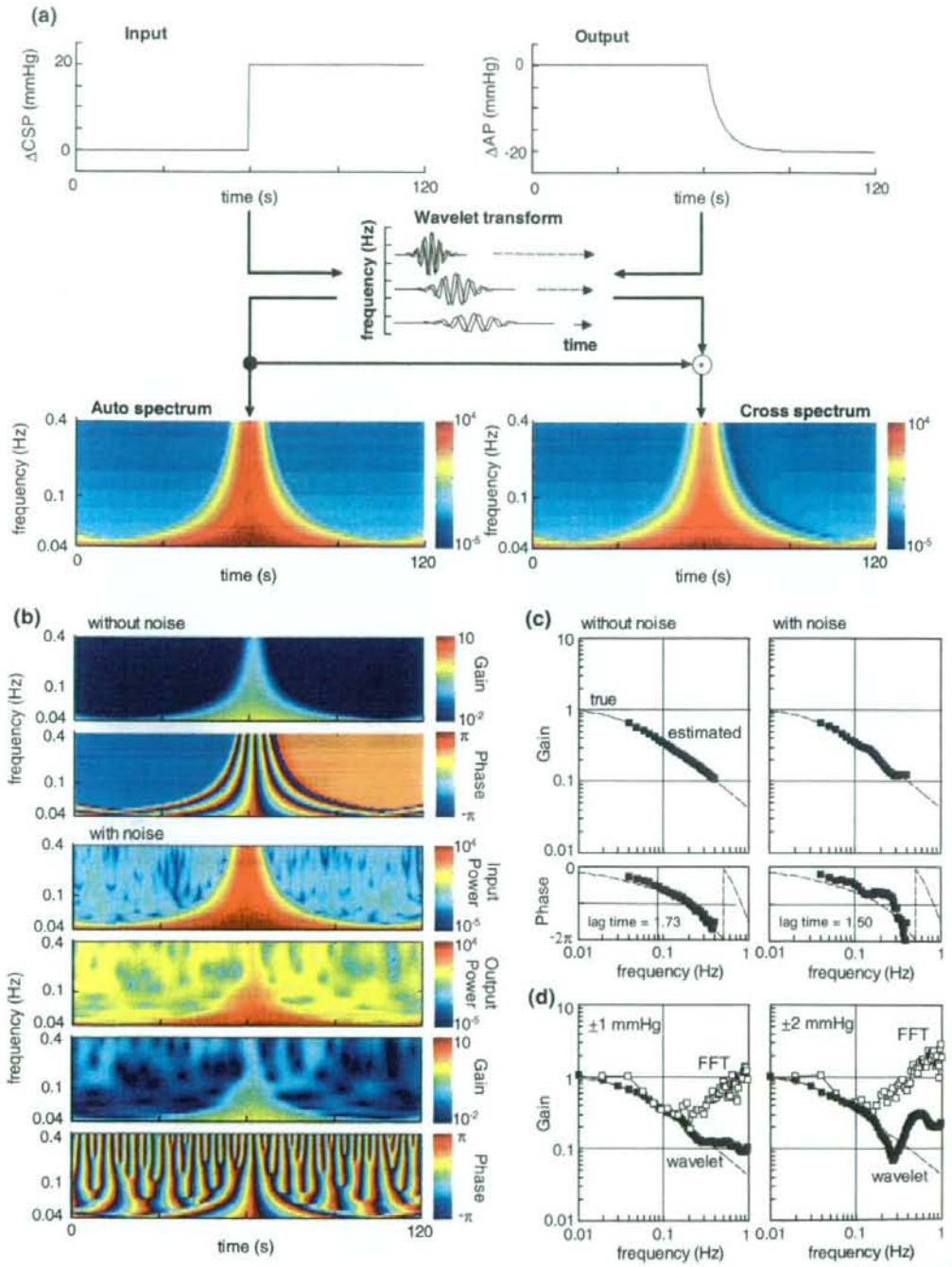

FIGURE 2. (a) Schematic illustration of the time-course system identification using wavelet analysis. The model response of total loop from CSP to AP under the carotid sinus open-loop condition was assessed for 120 s. Step input change of 20 mmHg was added to the system at 60 s. The time-series transfer function estimated by our wavelet analysis (b) and transfer function extracted from the time-course data of the total loop transfer function and the theoretical data (c). Gain (*top*) and phase (*bottom*) in the absence or presence of pseudo-random noise. (d) Gains in the short-time FFT and proposed wavelet analyses over wide frequencies (0.01–1 Hz) under the pseudo-random noise [±1 mmHg (*left*) and ±2 mmHg (*right*)].

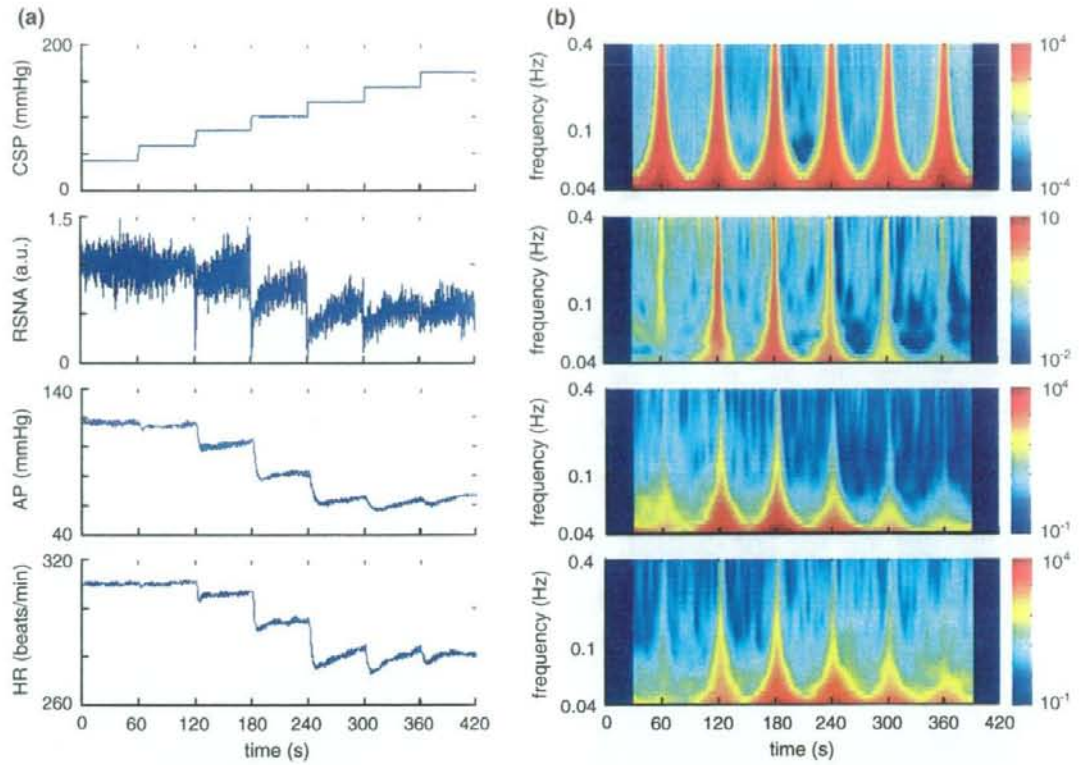

FIGURE 3. Averaged time series (a, $n = 8$) and wavelet power (b, $n = 8$) of CSP, renal sympathetic nerve activities (RSNA), AP, and heart rate (HR) during the static protocol. CSP was increased from 40 to 160 mmHg in 20 mmHg increments, resulting in changes of RSNA, AP, and HR through the carotid sinus baroreflex.

CSP_{40-60} and $CSP_{140-160}$ changes than other CSP changes.

Figure 5 and Table 1 show the average gain and phase ($n = 8$) in the neural arc (a), peripheral arc (b), total loop (c), and cardiac baroreflex (d). In the neural arc, $G_{0.04}$ (2.42 ± 0.07 a.u./mmHg) at the CSP_{80-100} change was the highest among all CSP changes, and was almost four to five times higher than those at the CSP_{40-60} (0.54 ± 0.09, $p < 0.01$) and $CSP_{140-160}$ (0.62 ± 0.06, $p < 0.01$) changes. Slopes increased significantly at lower and higher CSP changes compared with the $CSP_{100-120}$ change. Lag time at CSP_{80-100} was the shortest among all CSP changes. In the peripheral arc, Slope and lag time did not differ significantly among the CSP changes, whereas $G_{0.04}$ showed a tendency to decrease slightly with increase of CSP. In the total baroreflex, $G_{0.04}$ at CSP_{80-100} change (1.28 ± 0.12) was significantly higher compared to other CSP changes. Slopes were significantly greater at CSP changes within 60–120 mmHg than other CSP changes. Lag time did not differ significantly among CSP changes. In the cardiac baroreflex, $G_{0.04}$ (0.90 ± 0.18 and 0.92 ± 0.19 beats/min/mmHg) and Slopes were significantly higher at CSP_{80-100} and $CSP_{100-120}$ changes than other CSP changes. There were no significant differences in lag time among CSP changes.

Static Baroreflex

The static characteristics of the total loop were averaged ($n = 8$). Regression analysis was performed for logistic functions. Response range, coefficient of gain, midpoint of input axis, and minimum value of output were 0.45, 0.11, 99.6, and 0.55 in the neural arc, 65.2, 0.07, 97.6, and 69.4 in the total loop, and 29.5, 0.11, 98.2, and 281.2 in the cardiac baroreflex. Linear regression analysis was performed in the peripheral arc (static gain = 0.0086 and offset pressure = 0.027). The intersection between the CSP-AP curve and the line of identity corresponds to AP_{OP} (94.3 mmHg) located in the steepest portion (80–100 mmHg) of the sigmoid

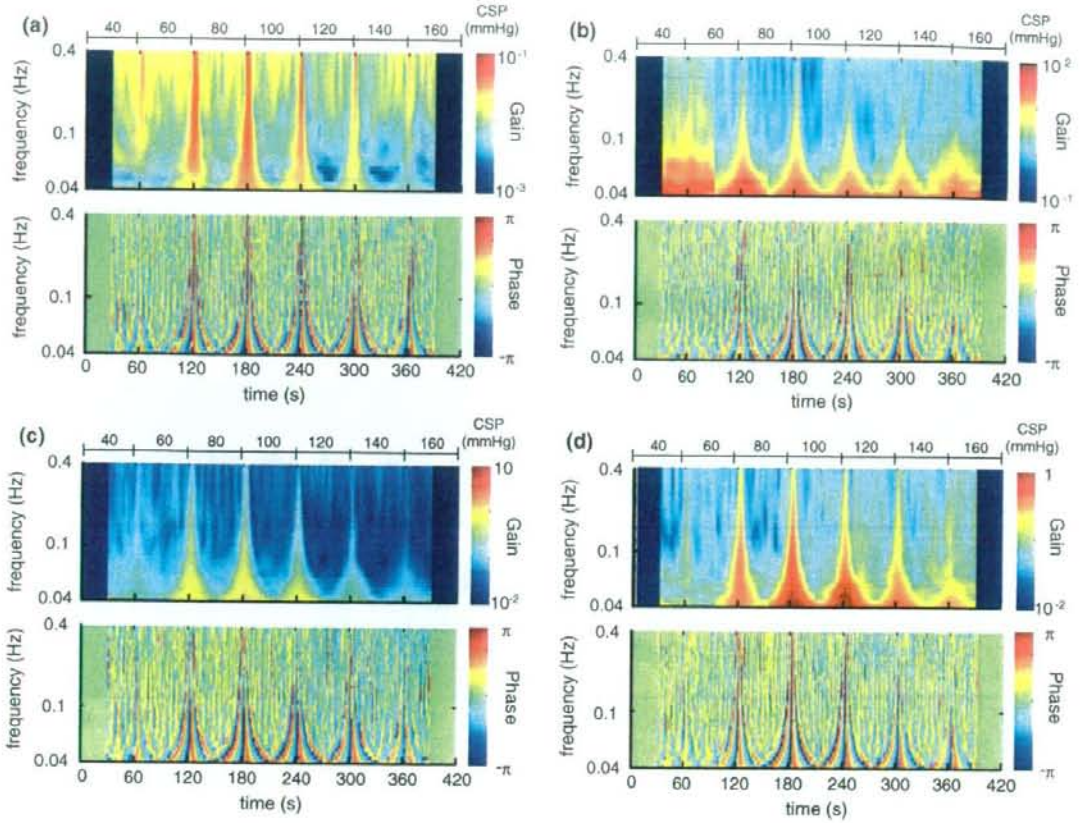

FIGURE 4. Time course of transfer functions of the neural arc from CSP to RSNA (a), peripheral arc from RSNA to AP (b), total baroreflex loop from CSP to AP (c), and cardiac baroreflex from CSP to HR (d) averaged across all animals ($n = 8$).

curve. In the equilibrium diagram, RSNA decreased with increasing CSP in the neural arc, AP increased with increasing RSNA in the peripheral arc, and the intersection between the two arcs provided the AP_{OP} (99.7 mmHg). In the cardiac baroreflex, HR decreased with the increase in CSP.

Bezold-Jarisch Reflex

In the total loop and cardiac baroreflex, the gains at various CSP changes during the BJR were identified ($n = 8$, Fig. 6 and Table 2). Averages of gain and phase (Fig. 6d) were derived from the time series in Figs. 6b and 6c. At middle CSP change of the total loop, $G_{0.04}$ was approximately halved under PBG condition compared to Control (0.59 ± 0.09 vs. 1.39 ± 0.15, $p < 0.01$). Slope and lag time did not differ significantly between the PBG and Control conditions at all CSP changes. In the cardiac baroreflex (Fig. 6e), $G_{0.04}$ tended to modulate under PBG condition at low and high CSP changes, but did not differ significantly between the two conditions at middle CSP changes. Slope differed significantly between the two conditions at low CSP change whereas lag time did not differ significantly at all CSP changes.

Cardiac Baroreflex

The ratio of the cardiac baroreflex to the total loop in dynamic characteristics was studied (Fig. 7). For CSP changes within 60–120 mmHg under Control condition, the ratios were almost linear and increased slightly with increase in frequency; in lower or higher CSP changes, they were modulated especially around 0.2 Hz. For CSP changes under PBG condition, overall the ratios were higher than those under Control condition. For CSP changes within 80–120 mmHg under PBG condition, the ratios were almost linear and the slopes were greater than those of Control condition; in lower or higher CSP changes, they

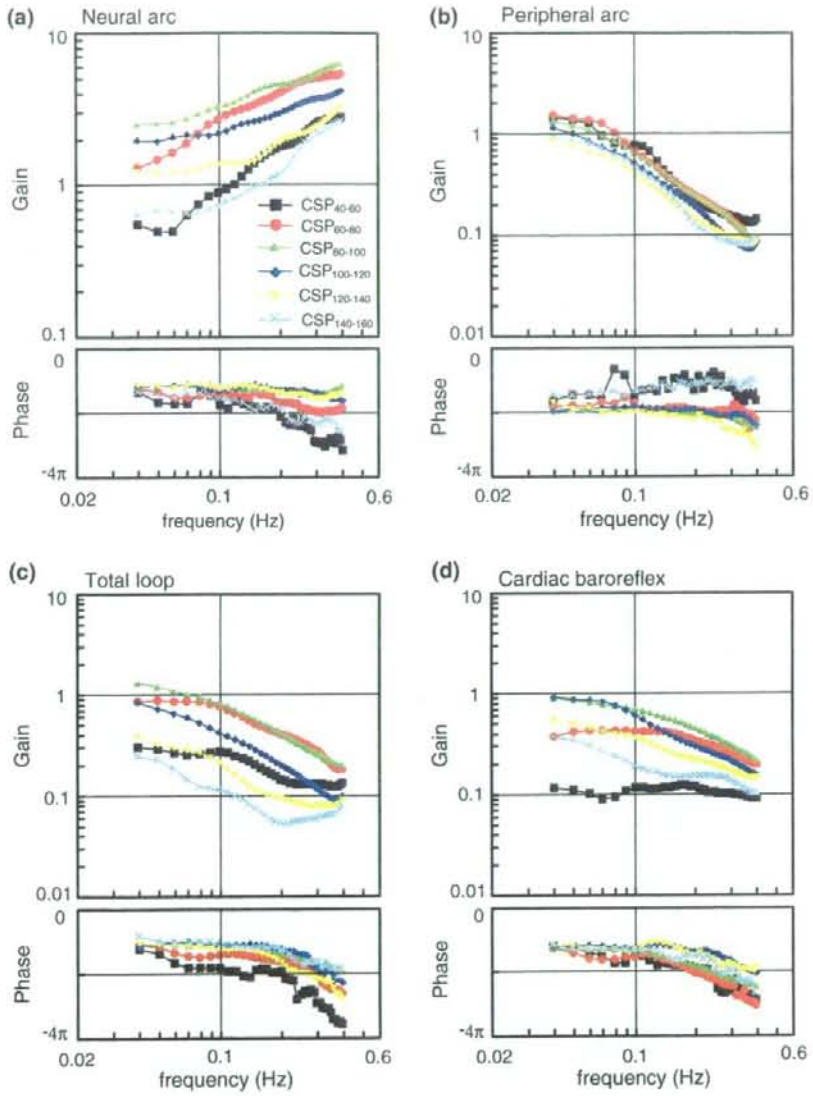

FIGURE 5. Transfer functions of the neural arc from CSP to RSNA, effective peripheral arc from RSNA to AP, total baroreflex loop from CSP to AP, and cardiac baroreflex estimated by wavelet analysis. Average (n = 8) gain (*top*) and phase (*bottom*).

increased within the 0.1–0.2 Hz range and decreased at higher frequencies. The phase difference did not differ among CSP changes under both Control and PBG conditions.

Closed-Loop Baroreflex

Simulation was performed using a cardiac baroreflex system from closed-loop AP input to HR output (Fig. 8a). To test the proposed wavelet analysis, an external disturbance to AP (AP_{noise} = +20 mmHg) was added to the system, and HR responses under carotid sinus open- and closed-loop AP responses were calculated (Fig. 8b). The observed AP and HR (AP_{change} and HR_{change}) were modulated by closed-loop regulation of AP. The CSP is identical with the observed AP_{change}. Gain and phase in the time series (Fig. 8c) and extracted (Fig. 8d) transfer functions were accurately estimated under open and closed AP responses.

TABLE 1. Parameters of the transfer functions in the neural arc, peripheral arc, total loop, and cardiac baroreflex at various step pressure inputs.

	CSP (mmHg)					
	40–60	60–80	80–100	100–120	120–140	140–160
Neural arc						
$G_{0.04}$ (a.u./mmHg)	0.54 ± 0.09	1.25 ± 0.17**	2.42 ± 0.07**,††	1.89 ± 0.13**,†	1.18 ± 0.20*,‡‡,**	0.62 ± 0.06†,‡‡,**
Slope (dB/decade)	17.9 ± 4.1	10.0 ± 1.9	7.7 ± 2.0	5.8 ± 3.1*	11.0 ± 1.8	16.8 ± 3.1*
Lag time (s)	2.63 ± 0.58	0.78 ± 0.16*	0.27 ± 0.18**	0.48 ± 0.14**	0.45 ± 0.17**	1.83 ± 0.71
Peripheral arc						
$G_{0.04}$ (mmHg/a.u.)	1.42 ± 0.17	1.50 ± 0.18	1.30 ± 0.08	1.13 ± 0.13	0.85 ± 0.10†	0.92 ± 0.09†
Slope (dB/decade)	−24.6 ± 3.3	−29.4 ± 1.3	−28.2 ± 0.8	−26.6 ± 2.8	−22.7 ± 2.8	−23.2 ± 4.6
Lag time (s)	0.40 ± 0.79	1.29 ± 0.20	1.35 ± 0.20	1.35 ± 0.58	2.10 ± 0.69	0.08 ± 0.64
Total loop						
$G_{0.04}$	0.29 ± 0.05	0.85 ± 0.16**	1.28 ± 0.12**,††	0.83 ± 0.09**,‡‡	0.38 ± 0.07††,‡‡,**	0.24 ± 0.04††,‡‡,**
Slope (dB/decade)	−6.8 ± 4.1	−19.4 ± 2.4**	−20.5 ± 1.6**	−20.7 ± 2.1**	−11.8 ± 2.7	−6.4 ± 4.1††,‡‡,**
Lag time (s)	3.03 ± 0.61	2.07 ± 0.12	1.62 ± 0.20	1.82 ± 0.60	2.54 ± 0.62	1.91 ± 0.41
Cardiac baroreflex						
$G_{0.04}$ (beats/min/mmHg)	0.11 ± 0.02	0.37 ± 0.11	0.90 ± 0.18**,††	0.92 ± 0.19**,††	0.55 ± 0.12**,‡,*	0.36 ± 0.09‡‡,**
Slope (dB/decade)	−2.3 ± 2.1	−10.7 ± 2.3	−15.9 ± 2.8**	−19.0 ± 2.9**	−11.8 ± 2.6	−6.3 ± 3.1‡,**
Lag time (s)	2.13 ± 0.62	2.26 ± 0.34	2.17 ± 0.62	1.51 ± 0.16	1.70 ± 0.61	1.92 ± 0.86

$G_{0.04}$, transfer gain at 0.04 Hz. Slope, average slope of transfer gain between 0.1 and 0.4 Hz.
$p < 0.01$; ** vs. 40–60, †† vs. 60–80, ‡‡ vs. 80–100, and ** vs. 100–120 mmHg in CSP change; the same symbols of a single show $p < 0.05$.

DISCUSSION

We have shown that the analysis using wavelet transform can identify the dynamic baroreflex properties at various pressure levels from the time-course data under normal (Fig. 5) and pathophysiological conditions (Fig. 6) with background noise. The results of the proposed analysis applied in animal experiments indicate the possibility of its use in the assessment of human baroreflex (Figs. 7 and 8).

Time-Series Analysis for Dynamic Baroreflex

Under the background noise added to the response model, the proposed analysis applied to step response was able to detect the dynamic baroreflex characteristics (Fig. 2). The standard spectral analysis under stationary conditions has high reliability in the baroreflex test, and uses longer data to cancel the noise[31,38] at various pressure inputs and lose the short-term and important changes. In direct calculation of the dynamic characteristics from the step input output data, the traditional time series analysis might also have a disadvantage under noise contamination, which may cause poor S/N ratio in the impaired baroreflex function of cardiac diseases.[41] The STFFT using time windows of a constant range for all frequencies was actually unable to catch the dynamic property especially at higher frequencies under such condition (Figs. 1 and 2d) because of the average one within the whole time window. On the other hand, the modified wavelet-based analysis with improved temporal resolution at higher frequencies to reasonably catch the localized changes in cardiovascular control[4,50] will be effective for extracting the dynamic baroreflex characteristics under nonstationary hemodynamics with a low S/N ratio. Because the baroreflex test may depend on the various S/N ratios depending on the system input (e.g. amplitude) and/or the background noises, further investigations will be required in this regard.

Burgess *et al.*[2] showed that cross spectrum analysis using wavelet transform characterized strong coupling between sympathetic nerve traffic and AP at frequencies of <0.1 Hz. Davrath *et al.*[4] reported that time-varying power obtained from wavelet transform of the spontaneous HR or AP fluctuation in humans are remarkably modulated at approximately 0.1 Hz under standing condition. Whereas the traditional wavelet analysis could extract the localized characteristics of time-series data in a nonstationary condition,[2,4] application to dynamic system identification is difficult because of the limitation in phase extraction. When the same time window is set for the input and output data, the actual information of phase and gain may be lost or split, instead of high temporal resolution of wavelet transform.[34] To apply wavelet analysis to the baroreflex system identification, we expanded the basic analysis by acquiring the transfer function from maximum input and output data. The proposed method was able to acquire the system identification of baroreflex because of the specific characteristics of wavelet

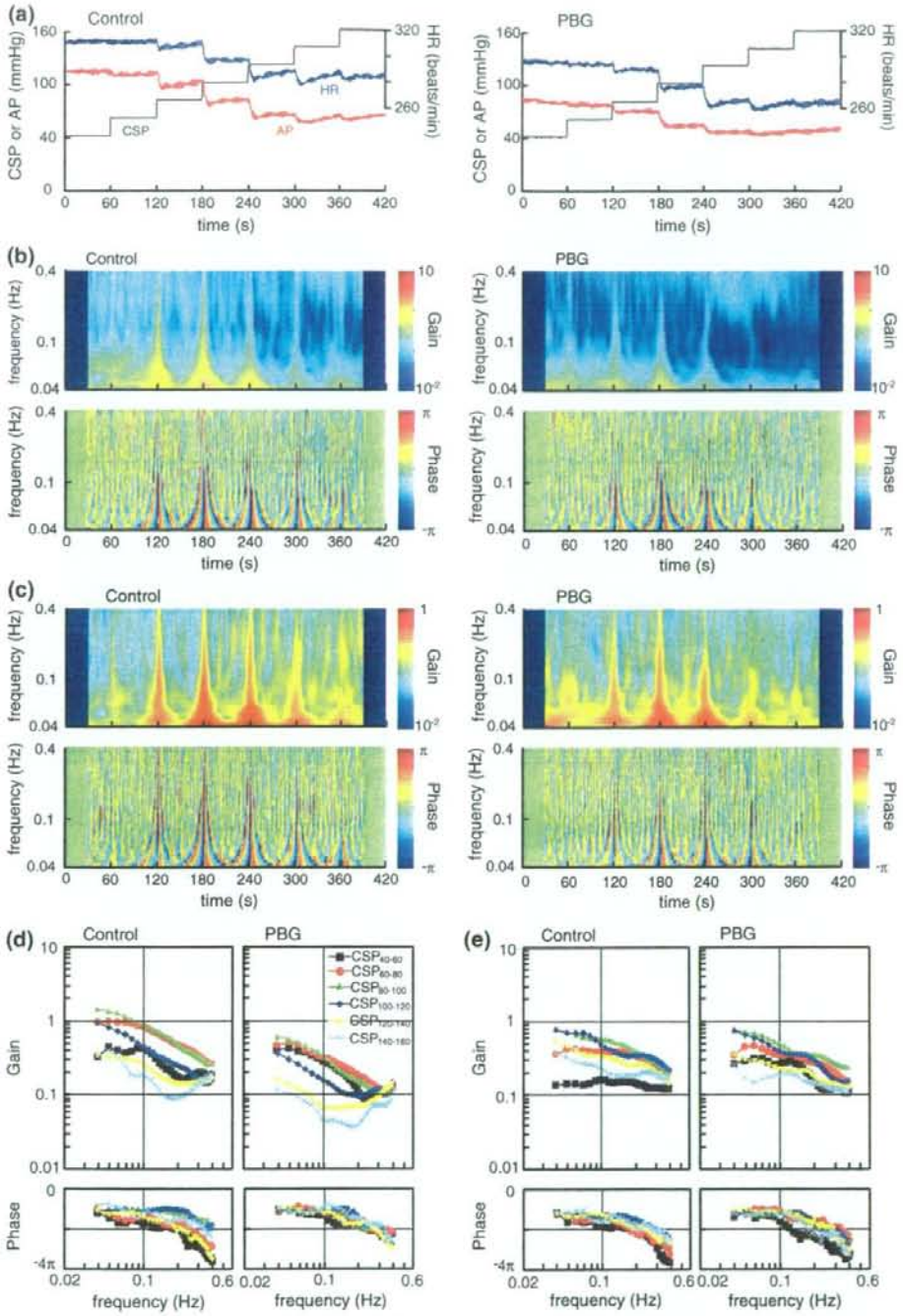

FIGURE 6. (a) Averaged (n = 8) time series of CSP, AP, and HR obtained in the absence (Control, *left*) and presence of phenylbiguanide (PBG, *right*). CSP was increased from 40 to 160 mmHg in 20 mmHg increments, resulting in changes in AP and HR through the carotid sinus baroreflex. Time-series transfer functions of total loop (b) and cardiac baroreflex (c) in the Control (*left*) and PBG (*right*) conditions. Average (n = 8) gain (*top*) and phase (*bottom*). Transfer functions of total loop (d) and cardiac baroreflex (e) estimated by wavelet analysis in the Control (*left*) and PBG (*right*) conditions.

TABLE 2. Parameters of the transfer functions for the total loop and cardiac baroreflex before and during PBG infusion.

	Low CSP (40–60 mmHg)		Middle CSP (80–100 mmHg)		High CSP (120–140 mmHg)	
	Control	PBG	Control	PBG	Control	PBG
Total loop						
$G_{0.04}$	0.32 ± 0.07	0.39 ± 0.09††	1.39 ± 0.15	0.59 ± 0.09**,††	0.35 ± 0.04††	0.15 ± 0.02††
Slope (dB/decade)	−11.6 ± 3.3	−8.0 ± 4.2	−17.8 ± 2.1	−15.0 ± 3.2	−6.5 ± 2.5	7.4 ± 5.3††
Lag time (s)	2.90 ± 0.71	1.43 ± 0.68	1.44 ± 0.22	2.21 ± 0.59	3.48 ± 0.61	2.74 ± 0.89
Cardiac baroreflex						
$G_{0.04}$ (beats/min/mmHg)	0.14 ± 0.02	0.26 ± 0.10†	0.78 ± 0.21	0.75 ± 0.18	0.54 ± 0.13	0.35 ± 0.08†
Slope (dB/decade)	−1.8 ± 2.2	−12.5 ± 2.9*	−13.4 ± 2.7	−11.6 ± 2.1	−12.6 ± 2.7	−6.6 ± 4.0
Lag time (s)	2.99 ± 0.89	2.91 ± 0.55	2.06 ± 0.30	2.28 ± 0.54	2.65 ± 0.72	2.47 ± 0.77

$G_{0.04}$, transfer gain at 0.04 Hz. Slope, average slope of gain between 0.1 and 0.4 Hz. PBG, phenylbiguanide.
** $p < 0.01$ and * $p < 0.05$, PBG vs. Control at the same CSP; †† $p < 0.01$ and † $p < 0.05$, all conditions vs. CSP_{80-100} of Control.

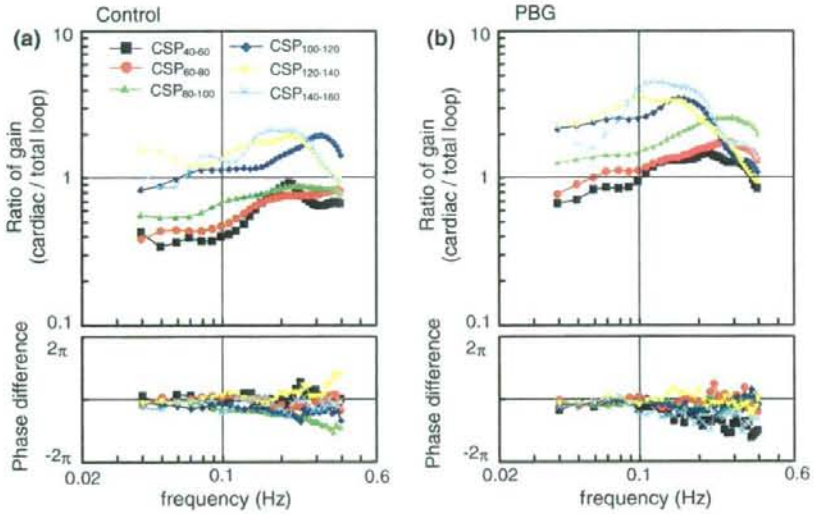

FIGURE 7. The ratio in the transfer functions of the cardiac baroreflex (CSP-HR) to the total loop (CSP-AP) (n = 8). The ratio of dynamic gain (*top*) and the phase difference (*bottom*). Control (a) and PBG (b) conditions.

transform that can adjust the analysis window at every frequency level and extract the localized data. When the mother wavelet is appropriately used for any purpose, the fields of the application of wavelet analysis might be extended. We used the traditional and reasonable Morlet function;[11,48,49] however, the comparison with other wavelet functions such as Mexican hat, Haar, and Daubechies[34] will be required in future studies. In addition, the convolutions within the transfer function of Eq. (3) may lose the temporal information; however, because the wavelet transform reflects the effect of reasonably changed time window, the gain and phase updated every 0.2 s can continuously express the representative property at the center point of the time window during the time-course change.

Physiological Perspective

The powers of the RSNA, AP, and HR responses to CSP changes showed maximum values at CSP_{80-100} change (Fig. 3b), which was almost consistent with AP_{OP} (94.3 and 99.7 mmHg) from static analysis. In contrast, the power responses at CSP_{40-60} and $CSP_{140-160}$ changes were lower than those at AP_{OP}, resulting from the nonlinear characteristics of the baroreflex around threshold and saturation to AP inputs as indicated by the static analysis. The gain and phase were revealed within the physiological range including nonlinear points in normal rabbits (Figs. 4 and 5). Whereas the static analysis cannot show the dynamic characteristics at higher frequencies (e.g. >0.01 Hz[18]), the proposed wavelet-based analysis

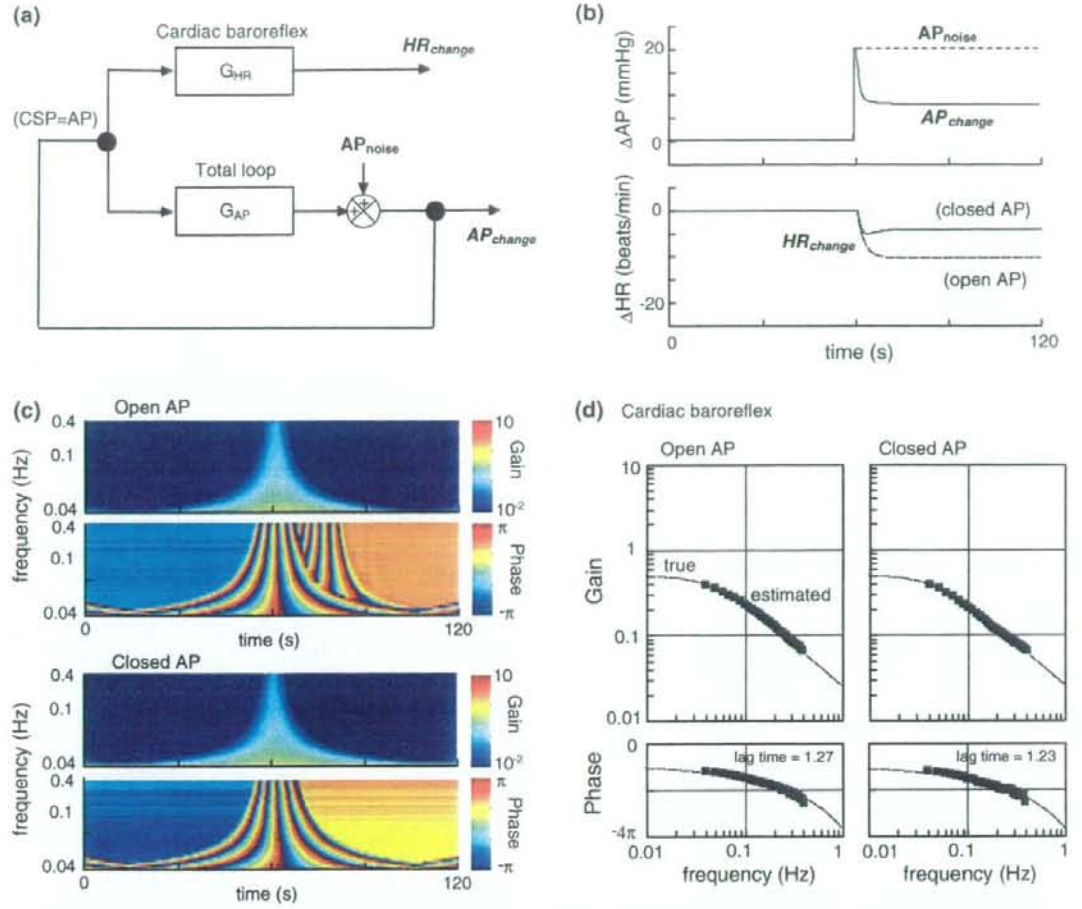

FIGURE 8. (a) Block diagram of cardiac baroreflex under closed-loop AP response. AP_{noise} indicates the external disturbance to AP. AP_{change} and HR_{change} show the actual changes of AP and HR. G_{AP} and G_{HR} are transfer functions under open loop responses in the total loop and cardiac baroreflex. (b) AP_{noise} of +20 mmHg as input and AP_{change} as output under the closed loop (*top*). HR responses under the open- and closed-loop AP changes (*bottom*). (c) Time-series transfer functions of cardiac baroreflex under open- and closed-loop AP changes. (d) Transfer functions of cardiac baroreflex estimated under the open (*left*) and closed (*right*) AP responses. Gain (*top*) and phase (*bottom*). Dotted lines, theoretical values. Squares, estimated values by our wavelet analysis.

could derive them from the same step input protocol, which may be able to reduce the number of experiments and duration of data acquisition.

Clinical Implications for Cardiac Patients

The wavelet-based system identification indicated a possibility to acquire pathophysiological understanding under various responses with cardiac diseases. The proposed analysis revealed that the dynamic characteristics in the total loop and neural arc were significantly attenuated at various pressure changes containing nonlinear points under PBG condition (Fig. 6 and Table 2), in addition to the previous studies.[18,20] The $G_{0.04}$ at AP_{OP} in Control (1.39 ± 0.15) was decreased to almost half during PBG condition (0.59 ± 0.09); it was attenuated to 1/3–1/4 times as small as that under PBG condition (0.39 ± 0.09) at low CSP_{40-60} change, which may be induced by the decrease of peripheral pump function in heart failure, suggesting the risk of further bluntness of baroreflex ability during the BJR.

In carotid-cardiac response, HR may be related to the assessment of AP regulation by the product of HR, stroke volume, and total peripheral resistance, rather than RR interval.[7,8] Because it may be difficult to evaluate the baroreflex to regulate AP under the carotid-sinus closed loop condition (i.e. CSP = AP), we

explored the possibility to evaluate the baroreflex dynamics from the HR response related to AP regulation, considering the dissociation between animal and human studies and applying the proposed method. The transfer functions of the cardiac baroreflex were similar to those of the total loop around the operating point (Fig. 7a). On the other hand, the dynamic characteristics in nonlinear CSP points and during the BJR were greater than those around the operating point in Control condition (Fig. 7b), suggesting the effect of cardiac sympathovagal activity. Next, to consider human baroreflex assessment, the dynamic transfer function was estimated by the closed-loop model response (Fig. 8), resulting in the effective assessment. Even when the system input is modulated by the nature of closed-loop response, it would be crucial to be able to estimate the dynamic baroreflex characteristics.

The spontaneous baroreflex method is commonly used in clinical assessments.[37] This method may have some limitations because of the highly complex and interconnected cardiovascular mechanisms in short-term AP regulation[27,40,43] and the unclear system input might induce the different pathophysiological understandings.[42] On the other hand, our focus was to explore the possibility of the evaluation of the baroreflex to regulate AP against great external disturbances in patients with cardiovascular diseases and unstable hemodynamics. To identify the system dynamics of the carotid-sinus baroreflex for AP regulation with sympathovagal activity,[51] this study improved the standard analyses, particularly considering the pure time delay. Using the transfer function corresponding to the independent step input frequency, the proposed analysis was able to indicate some novel aspects of the dynamic baroreflex properties during the BJR as mentioned above.

For clinical application, the other indexes (e.g. AP to muscle SNA response[14]) for AP regulation might be tested. In addition, in the time-course data, there are some effective methods such as complex demodulation method[13] based on the low pass filter, focusing on a frequency band such as LF and HF; it has good temporal resolution. However, the complex demodulation method might concentrate on the information of amplitude in a frequency band, not on each frequency level within the band. This limitation makes it impossible to perform the system identification in this study to reproduce the response corresponding to a wide frequency. Furthermore, the continuous estimation of the dynamics might connect to an effective index of the real-time control of hemodynamics such as an automated drug infusion system.[17,19]

Because we kept the bilateral vagi intact, low pressure baroreflexes from the cardiopulmonary region might have interacted with the arterial baroreflex, affecting estimation of carotid sinus baroreflex transfer functions. After the vagotomy, the dynamics from isolated aortic depressor nerve to AP responses was almost preserved and AP remained unchanged despite a HR decrease.[28,46] Our previous data of dynamic baroreflex properties with[20] and without[21] vagal nerves were compared. The dynamic characteristics of the total loop and cardiac baroreflex around the operating point were similar, whereas the corner frequency was slightly greater under intact vagal condition. Next, the static gain may be increased during the rising pressure protocol, compared with the falling one.[46] Hysteresis induced by the rising and falling pressure protocols may also modulate the dynamic baroreflex. However, the vagal effect of the cardiovascular receptors on the dynamics may not be large.[28] Third, the phases at lower or higher CSP changes in the transfer functions varied with the observed frequency because of nonlinear characteristics in the neural arc and the input power in the peripheral arc decreased by the neural arc. Especially at high frequencies, the phases appear to be modulated because of the step input showing low power with the high frequency. Finally, the simple models used for the simulations in this study have some limitations, such as a lack of information of nonparametric components or nonlinearity.[23]

CONCLUSIONS

The wavelet-based time-frequency analysis was capable of identifying the dynamic baroreflex properties over wide frequencies at various pressure levels both in normal and BJR conditions. Because the dynamic baroreflex properties to physiological pressure inputs as well as static characteristics can be simultaneously extracted from the short-term responses with background noise, the proposed method is potentially applicable to assess human dynamic baroreflex function under carotid-sinus closed-loop condition.

APPENDIX

Model Response of Arterial Baroreflex

We used the following model[15] as the carotid sinus open loop baroreflex for the simulation study (Figs. 1 and 2). The neural arc transfer function $[G_N(f)]$ using a first-order high-pass filter can be expressed as

$$G_N(f) = -K_N\left(1 + \frac{f}{f_C}i\right)\exp(-2\pi f i L_N)$$